

Dielectron production in 200 GeV p+p and Au+Au collisions at STAR

Yi Guo for the STAR collaboration

E-mail: yiguo@rcf.rhic.bnl.gov

Abstract. Leptons do not interact strongly with the hot dense medium created in relativistic heavy ion collisions. They can escape the interaction region undistorted and thus carry direct information about the space-time evolution of the expanding system. In the low mass region (LMR, $0.3 < M_{ee} < 1.1$ GeV/ c^2), dielectron mass spectra can provide the in-medium vector meson properties, while in the intermediate mass region (IMR, $1.1 < M_{ee} < 3$ GeV/ c^2), the slope of dielectron transverse mass spectra is expected to have connection with the QGP temperature.

In this paper, we present the centrality and p_T dependence of the dielectron mass spectra measured in STAR experiment at RHIC. The data sets used in the analysis include large statistics samples collected during years 2010 for 200 GeV Au+Au collisions and 2012 for 200 GeV p+p collisions. In order to extract underlying physics, we will compare our results with model calculations.

1. Introduction

Dileptons are clean and penetrating probes for the hot and dense nuclear matter created by the high energy nuclear collisions because they do not suffer from strong interactions. They can be produced during all stages of a heavy ion collision, and their sources are expected to have different contributions to dilepton invariant mass spectra. Therefore, a systematic measurement of the dilepton pair distribution can reveal the properties of medium created by high energy nuclear collisions.

Dilepton measurements have been pursued for decades in heavy ion collisions [1]-[7]. The CERES measurement of e^+e^- mass spectra showed a clear enhancement in the mass region below ~ 0.7 GeV/ c^2 compared to the known hadronic sources [4]. High precision data from NA60 suggested that this enhancement is consistent with in-medium broadening of the ρ spectral function instead of a dropping of its pole mass hypothesis [5], [8]-[11]. In addition, slope parameters of dimuon transverse mass spectra showed a sudden drop above the ϕ mass after removing the correlated charm contributions. This is argued to be an indication of thermal dilepton from partonic source by the NA60 collaboration [6]. At RHIC energy, the result from PHENIX showed a significant enhancement in mass region $0.3 \sim 0.76$ GeV/ c^2 [7]. However, the huge enhancement could not be reproduced by those model calculations which successfully explained SPS data [8]-[11].

In this paper, we will present the newest STAR results on dielectron production from 200 GeV p+p and Au+Au collisions, and compare the Au+Au results with model calculations.

2. Analysis

Data used in the analysis are obtained from 200 GeV p+p and Au+Au collisions, which were collected by the Solenoidal Tracker At RHIC (STAR) detector [12] in year 2012 and year 2010, respectively. The main subsystems used in the analysis are Time Projection Chamber (TPC) [13] and the Time of Flight (TOF) [14].

In addition of track reconstruction and momentum information, TPC also provides identification capabilities for charged particles by their ionization energy loss (dE/dx) in the TPC gas. With the fully installed TOF system, the PID capabilities are greatly improved, especially in low p_T region. With the combination of dE/dx from TPC and velocity (β) from TOF, the electron purity is $\sim 98\%$ in p+p collisions, $\sim 95\%$ in Au+Au minimum bias collisions and $\sim 93\%$ in Au+Au central collisions.

Two methods were used in this analysis to reconstruct the background. In LMR, due to the correlated background, e.g. cross pair and jet contribution, we used the like-sign method background with an acceptance correction. The acceptance correction is to account for the slight difference in the acceptance between like-sign and unlike-sign pairs [15]. While in IMR, the mix-event technique was used to achieve better statistics. The difference between these two methods were taken as systematic uncertainty. Figure 1 left panel (a) shows the raw dielectron mass distribution, reconstructed background and signal after background subtraction in 200 GeV Au+Au minimum bias collisions. The signal-to-background ratios from p+p minimum bias collisions, Au+Au minimum bias and central collisions are shown in Fig. 1 left panel (b). In this analysis, we also subtracted the contribution from the photon conversion by the method used in Ref. [16].

The dielectron continuum results in this paper were obtained in STAR acceptance ($p_T^e > 0.2$ GeV/c, $|\eta^e| < 1.0$, $|y^{ee}| < 1.0$) and corrected for the efficiency.

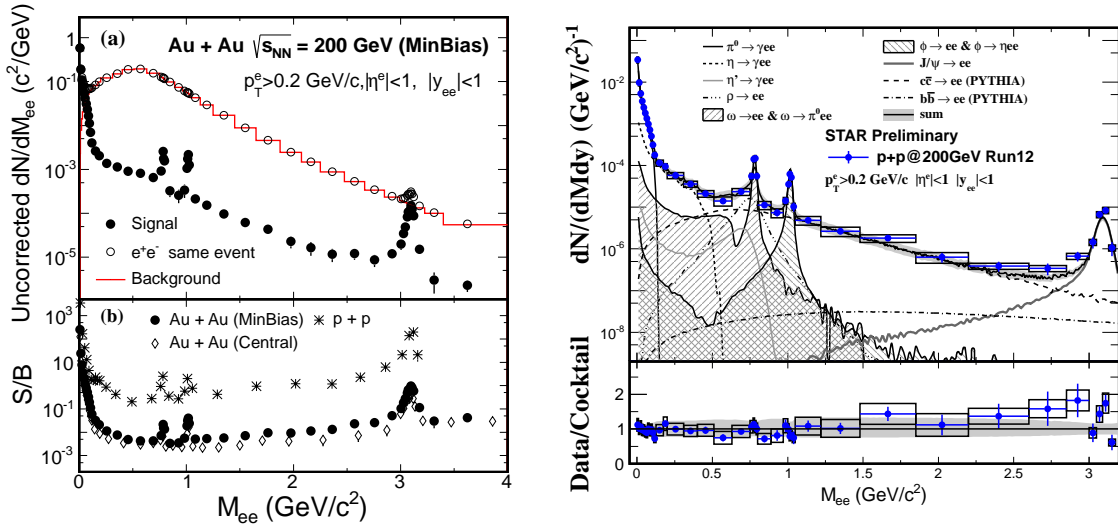


Figure 1. Left panel (a): e^+e^- raw invariant mass distribution (open circles), the reconstructed backgrounds (red histogram) and the signal (solid dots) in 200 GeV Au+Au minimum bias collisions [18]. Left panel (b): The signal to background ratio in p+p and Au+Au collision at $\sqrt{s_{NN}} = 200$ GeV [18]. Right panel: invariant mass spectra from $\sqrt{s} = 200$ GeV p+p collisions taken from year 2012. The black open box represents systematic error from data while the grey band depicts systematic uncertainty of cocktail.

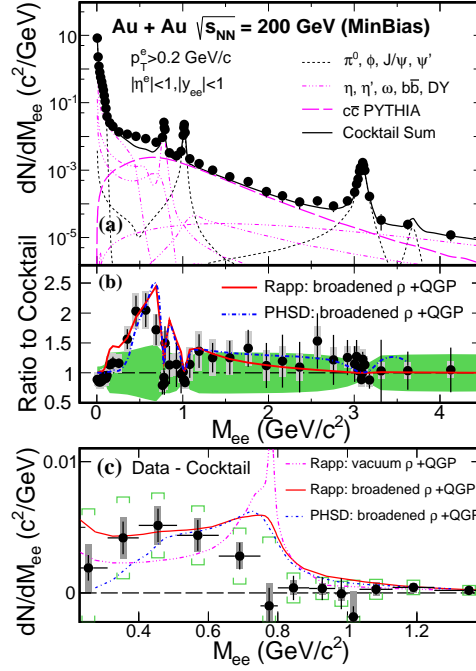


Figure 2. (a) Invariant mass spectra, (b) ratio of data to cocktail and (c) excess spectra in LMR from $\sqrt{s_{NN}} = 200$ GeV Au+Au minimum bias collisions [18]. Two model calculations are also included. In panel (b), the grey box represents the systematic uncertainty from data while the light green band shows the systematic uncertainty from cocktail. In panel (c), green brackets depict the total systematic uncertainties including those from cocktail.

3. Results

Figure 1 right panel shows the dielectron invariant mass spectra from 200 GeV p+p collisions taken in year 2012. The cocktail is taken from the STAR published result [15], and the charm cross section is updated to $797 \pm 210(\text{stat.})^{+208}_{-295}(\text{sys.})\mu\text{b}$ with respect to the newest published result from STAR [17]. The cocktail simulation can reproduce the new preliminary result very well. With a full TOF coverage and more data taken, year 2012 result has greatly improved statistics which is ~ 7 times more than STAR published result [15]. The large statistics new results at p+p 200 GeV provide a better baseline for Au+Au collisions.

The $\sqrt{s_{NN}} = 200$ GeV Au+Au results taken in year 2010 has been accepted by Phys.Rev.Lett [18]. In this paper, we will briefly review the key content of the submitted paper.

In LMR, an enhancement of $1.77 \pm 0.11(\text{stat.}) \pm 0.24(\text{sys.}) \pm 0.41(\text{cocktail})$ is observed with respect to the cocktail without ρ , in the mass region $0.3 \sim 0.76$ GeV/c^2 in minimum bias collision (Fig. 2 (b)). In addition, two model calculations [19, 20] are included to compare with our data (Fig. 2 (b), (c)): Model I by Rapp *et al.* is an effective many-body calculation [8, 19]; Model II by Linnyk *et al.* is a microscopic transport model, Parton-Hadron String Dynamics (PHSD) [11, 20]. Both models involve in-medium broadened ρ spectral function hypothesis and can successfully reproduce the NA60 results. The models, however, failed to reproduce the enhancement in central collisions reported by the PHENIX experiment [7, 20]. In the mass region below 1 GeV/c^2 , both models describe our data reasonably well within uncertainties. Our measurements disfavor a pure vacuum ρ mass distribution for the excess dielectron ($\chi^2/NDF = 25/8$ in 0.3-1 GeV/c^2 , Fig. 2 (c)).

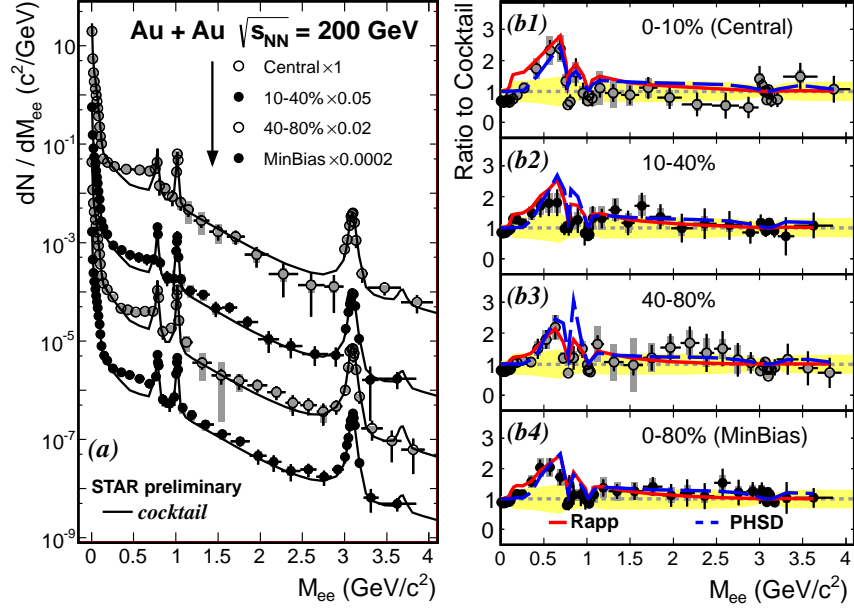


Figure 3. Left panel shows dielectron invariant mass spectra in different centralities. The solid curves represent the hadronic cocktail. The charm contribution is calculated by PYTHIA and scaled by N_{bin} . Right panel shows the ratio of data to cocktail in different centralities. The yellow band represents the systematic uncertainty of cocktail.

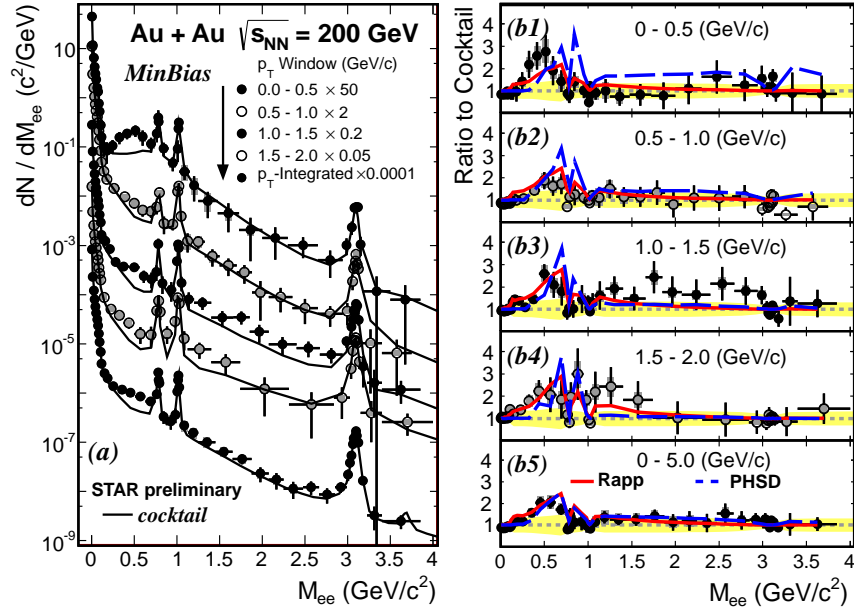


Figure 4. Left panel shows dielectron invariant spectra in different p_T^{ee} ranges. The solid curves represent the hadronic cocktail. Right panel shows the ratio of data to cocktail in different p_T^{ee} ranges. The yellow band represents the systematic uncertainty of cocktail.

Figures 3 and 4 show the dielectron spectra measured in various centrality bins and p_T

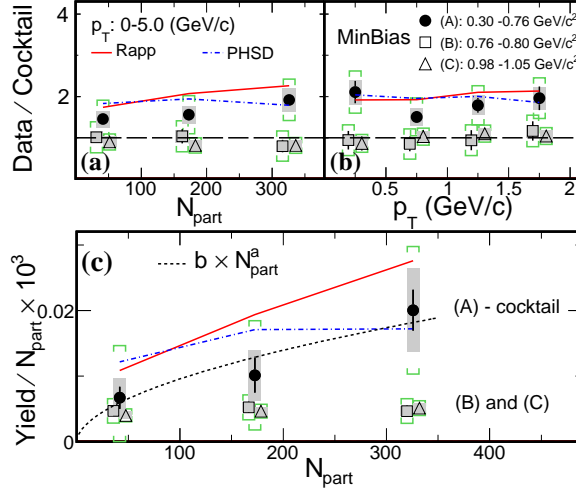


Figure 5. Panel (a) and (b) shows the integrated dielectron yields in mass regions of 0.3-0.76(ρ -like), 0.76-0.80(ω -like) and 0.98-1.05(ϕ -like) GeV/c^2 as a function of centrality and p_T^{ee} . Panel (c) shows the yields scaled by N_{part} for the ρ -like with cocktail subtraction, and the ω -like and ϕ -like without cocktail subtraction [18]. The dashed curve is a power-law fit to the yield/ N_{part} for the ρ -like region subtracted by cocktail. Systematic uncertainties from data are shown as grey boxes, while the green brackets represent the total systematic uncertainties including the cocktail contribution. The ω -like and ϕ -like data points are slightly displaced horizontally for clarity.

ranges, respectively. The ratios between data and cocktail are shown in the right panels. Model calculations are also included as a comparison. Both models are able to describe the LMR excess in all p_T and centrality bins within uncertainty.

We also report the ratios of data to cocktail within STAR acceptance in three different mass regions: 0.3-0.76 (ρ -like), 0.76-0.8(ω -like) and 0.98-1.05(ϕ -like) GeV/c^2 as a function of centrality Fig. 5 (a) and dielectron p_T Fig. 5 (b). The hadronic cocktail can reproduce the dielectron yield in the ω -like and ϕ -like regions. In the ρ -like region, a significant excess is observed and the ratio of data to cocktail shows a weak dependence on N_{part} and dielectron p_T . Figure 5 (c) shows the yields in the ρ -like region subtracted by cocktail, and the ω -like and ϕ -like regions without cocktail subtraction. Dielectron yields in the ω -like and ϕ -like regions show a N_{part} scaling. The dashed curve is a power fit ($\propto N_{\text{part}}^a$) to the excess yield/ N_{part} in the ρ -like region, and the fit result shows $a = 0.54 \pm 0.18$ (stat.+uncorrelated sys.), indicating the dielectron excess yields in the ρ -like region are sensitive to the QCD medium dynamics, as expected by the theoretical calculations [19, 21].

In Fig. 6, we overlay the dielectron mass spectra from minimum bias and most central (0-10%) collisions. The spectra are scaled by the number of participant nucleons (N_{part}). The ratio in the bottom panel starts from unity in the π^0 and η mass region and begins to increase in mass region 0.5-1 GeV/c^2 towards the N_{bin} . This is due to the fact that correlated charm contribution starts to dominate in this mass region and the charm quark production at RHIC energy is expected to follow the N_{bin} scaling. The hadronic medium also has a significant contribution in this mass region and is expected to increase faster than N_{part} [19, 21]. In the IMR region, the ratio shows a moderate deviation from the N_{bin} scaling (1.8σ deviation for the data point at 1.8-2.8 GeV/c^2). The difference in mass region 1-3 GeV/c^2 indicates a potential de-correlating effect on charm pairs while traversing the QCD medium or other contribution from medium (e.g thermal radiation).

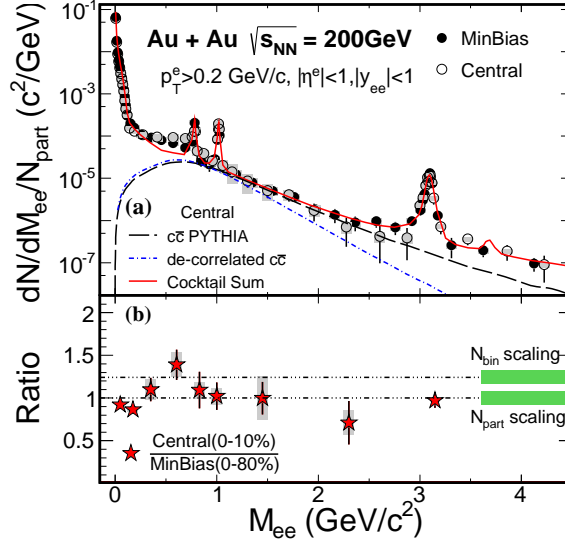


Figure 6. (a) Dielectron invariant mass spectra from minimum bias (0-80%) and central (0-10%) collisions [18]. The spectra are scaled by the number of participant nucleons (N_{part}). The solid line represents the hadronic cocktail for central collisions. The dashed line depicts the correlated charm from PYTHIA, while the dot-dashed line assumes a fully randomized azimuthal correlation between charm pairs and the p_T suppression factor on single electron spectrum from RHIC is also included [22]. (b) The ratio of N_{part} scaled dielectron yields between the central and minimum bias collisions. Systematic uncertainties are shown as the grey bands.

References

- [1] R.J. Porter *et al.*, Phys. Rev. Lett. **79**, 1229 (1997).
- [2] G. Adamova *et al.*, Phys. Rev. Lett. **98**, 052302 (2007); Phys. Rev. C **84**, 014902 (2011).
- [3] A.L.S Angelis *et al.*, Eur. Phys. J. C **13**, 433 (2000).
- [4] G. Agakichiev *et al.*, Phys. Rev. Lett. **91**, 042301 (2003); Eur. Phys. J. C **41**, 475 (2005).
- [5] R. Arnaldi *et al.*, Phys. Rev. Lett. **96**, 162302 (2006); Phys. Rev. Lett. **100**, 022302 (2008);
- [6] R. Arnaldi *et al.*, Eur. Phys. J. C **59**, 607 (2009).
- [7] A. Adare *et al.*, Phys. Rev. C **81**, 034911 (2010).
- [8] H. van Hees and R. Rapp, Phys. Rev. Lett. **97**, 102301 (2006); H. van Hees and R. Rapp, Nucl. Phys. A **806**, 339 (2008).
- [9] J. Ruppert, C. Gale, T. Renk, P. Lichard and J. Kapusta, Phys. Rev. Lett. **100**, 162301 (2008); T. Renk and J. Ruppert, Phys. Rev. C **77**, 024907 (2008).
- [10] K. Dusling, D. Teaney and I. Zahed, Phys. Rev. C **75**, 024908 (2007).
- [11] O. Linnyk *et al.*, Phys. Rev. C **84**, 054917 (2011).
- [12] Special Issue on RHIC and Its Detectors, edited by M. Harrison, T. Ludlam, and S. Ozaki, Nucl. Instr. Meth. A **499**, No. 2-3 (2003).
- [13] M. Anderson, *et al.*, Nucl. Instr. Meth. A **499**, 659 (2003).
- [14] W.J. Llope (for the STAR Collaboration), Nucl. Instr. Meth. A **661**, S110 (2012).
- [15] L. Adamczyk *et al.*, Phys. Rev. C **86**, 024906 (2012).
- [16] A. Adare *et al.*, Phys. Rev. C **81**, 034911 (2010).
- [17] L. Adamczyk *et al.*, Phys. Rev. D **86**, 072013 (2012).
- [18] L. Adamczyk *et al.*, arXiv:1312.7397.
- [19] R. Rapp, PoS CPOD2013, 008 (2013); R. Rapp, private communications.
- [20] O. Linnyk *et al.*, Phys. Rev. C **85**, 024910 (2012); O. Linnyk, private communications.
- [21] U. Heinz and K.S. Lee, Phys. Lett. B **259**, 162 (1991).
- [22] A. Adare *et al.*, Phys. Rev. Lett. **98**, 172301 (2007).